Applied Physics Letters

Operating in a deep underground facility improves the locking of gradiometric fluxonium qubits at the sweet spots

Cite as: Appl. Phys. Lett. **120**, 054001 (2022); https://doi.org/10.1063/5.0075909
Submitted: 19 October 2021 • Accepted: 17 January 2022 • Published Online: 02 February 2022

Daria Gusenkova, Francesco Valenti, Martin Spiecker, et al.

Operating in a deep underground facility improves the locking of gradiometric fluxonium qubits at the sweet spots

Cite as: Appl. Phys. Lett. **120**, 054001 (2022); doi: 10.1063/5.0075909
Submitted: 19 October 2021 · Accepted: 17 January 2022 ·
Published Online: 2 February 2022

Daria Gusenkova,[1,2] Francesco Valenti,[1] Martin Spiecker,[1,2] Simon Günzler,[1] Patrick Paluch,[1,2] Dennis Rieger,[2] Larisa-Milena Pioraş-Ţimbolmaş,[3,4] Liviu P. Zârbo,[3] Nicola Casali,[5] Ivan Colantoni,[5,6] Angelo Cruciani,[5] Stefano Pirro,[7] Laura Cardani,[5] Alexandru Petrescu,[8] Wolfgang Wernsdorfer,[1,2] Patrick Winkel,[1] and Ioan M. Pop[1,2,a)]

AFFILIATIONS

[1]IQMT, Karlsruher Institute of Technology, Eggenstein-Leopoldshafen, Germany
[2]PHI, Karlsruhe Institute of Technology, Karlsruhe, Germany
[3]CETATEA, National Institute for Research and Development of Isotopic and Molecular Technologies, Cluj-Napoca, Romania
[4]Faculty of Physics, Babeş-Bolyai University, Cluj-Napoca, Romania
[5]INFN, Sezione di Roma, Roma, Italy
[6]CNR, Istituto di Nanotecnologia, c/o Dip. Fisica, Sapienza Università di Roma, Roma, Italy
[7]INFN Laboratori Nazionali del Gran Sasso, Assergi (AQ), Italy
[8]Institut Quantique and Département de Physique, Université de Sherbrooke, Sherbrooke, Canada

Note: This paper is part of the APL Special Collection on Emerging Qubit Systems - Novel Materials, Encodings and Architectures.
[a)]**Author to whom correspondence should be addressed:** ioan.pop@kit.edu

ABSTRACT

We demonstrate flux-bias locking and operation of a gradiometric fluxonium artificial atom using two symmetric granular aluminum (grAl) loops to implement the superinductor. The gradiometric fluxonium shows two orders of magnitude suppression of sensitivity to homogeneous magnetic fields, which can be an asset for hybrid quantum systems requiring strong magnetic field biasing. By cooling down the device in an external magnetic field while crossing the metal-to-superconductor transition, the gradiometric fluxonium can be locked either at 0 or $\Phi_0/2$ effective flux bias, corresponding to an even or odd number of trapped fluxons, respectively. At mK temperatures, the fluxon parity prepared during initialization survives to magnetic field bias exceeding $100\,\Phi_0$. However, even for states biased in the vicinity of $1\,\Phi_0$, we observe unexpectedly short fluxon lifetimes of a few hours, which cannot be explained by thermal or quantum phase slips. When operating in a deep-underground cryostat of the Gran Sasso laboratory, the fluxon lifetimes increase to days, indicating that ionizing events activate phase slips in the grAl superinductor.

The unique properties of the superconducting state emerging in a select list of materials below the critical temperature T_c have already been used for particle detection,[1–4] quantum-limited amplification,[5–7] quantum information processing,[8,9] and hybrid mesoscopic hardware.[10] While the main benefits offered by the superconducting state are unarguably its intrinsically low dissipation and the possibility to engineer strongly non-linear elements, such as Josephson junctions (JJs), another potential resource emerges as a consequence of the magnetic field quantization in superconducting loops and the associated long-lived persistent currents.[11,12] In classical superconducting circuits, trapped flux quanta called fluxons have been used for more than two decades in the so-called rapid single flux-quantum electronics[13,14] and might constitute a valuable resource for local magnetic field biasing in superconducting quantum processors.[15] In the quantum regime, fluxons have recently been proposed as a resource for quantum simulators.[16,17]

A prominent example for fluxon dynamics is the fluxonium qubit in which the tunneling of a fluxon through a JJ shunted by a superinductor[18–20] determines the eigenenergies and wavefunctions of the system.[21] In addition to the large anharmonicity of its energy spectrum, enabling fast operation, the fluxonium exhibits a so-called sweet spot with a long energy relaxation time and slow dephasing when the magnetic flux enclosed in the loop is half a flux quantum.[22,23]

In our device, we use an additional superinductor made from a superconducting granular aluminum (grAl)[25,26] thin film shunting the single Al-AlOx-Al JJ to build a fluxonium artificial atom with a gradiometric loop geometry, as shown in Fig. 1. As a result, our device has three loops in total: an outer loop entirely formed by superinductors and two inner loops, which are connected by a JJ weak link enabling quantum tunneling of fluxons between them. Similar to other gradiometric devices,[27,28] this loop geometry highly reduces the circuit's sensitivity to global magnetic fields, in our device by two orders of magnitude. This feature opens the way for its use in hybrid systems[29,30] where a large magnetic field is required to bias other quantum degrees of freedom, for instance, electronic spins in semiconducting heterostructures[31,32] or molecular qubits.[33,34]

The ground state for a superconducting loop threaded by a perpendicular external magnetic field involves a non-zero current, also known as persistent current, if the magnetic flux enclosed in the loop is not an integer multiple of the magnetic flux quantum $\Phi_0 = h/(2e)$. Similar to the Meissner effect, persistent currents can be induced by a static magnetic field if the superconducting loop is cooled below T_c and crosses the metal-to-superconductor phase transition. When the magnetic field is ramped down at temperatures well below T_c, the changing magnetic field induces a screening current such that the number of trapped flux quanta in the loop remains constant.[19]

We demonstrate that our grAl gradiometric fluxonium can be initialized at the half-flux sweet spot by cooling down through T_c in a static magnetic field corresponding to $1\,\Phi_0$ in the outer loop. From pulsed time-domain measurements, we find an average energy relaxation time of $T_1 = 10.0 \pm 0.3\,\mu s$ and a coherence time $T_2^* = 0.59 \pm 0.02\,\mu s$. Since the echo time $T_2 = 5.3 \pm 0.3\,\mu s$ is roughly an order of magnitude larger, we infer that our device is limited by local low-frequency noise of unknown origin, qualitatively consistent with previous observations.[35]

Although the grAl superinductor is expected to have an extremely low phase-slip rate $\sim 10^{-20}$ Hz, we only observe a lifetime of the persistent current on the order of hours in a typical setup not

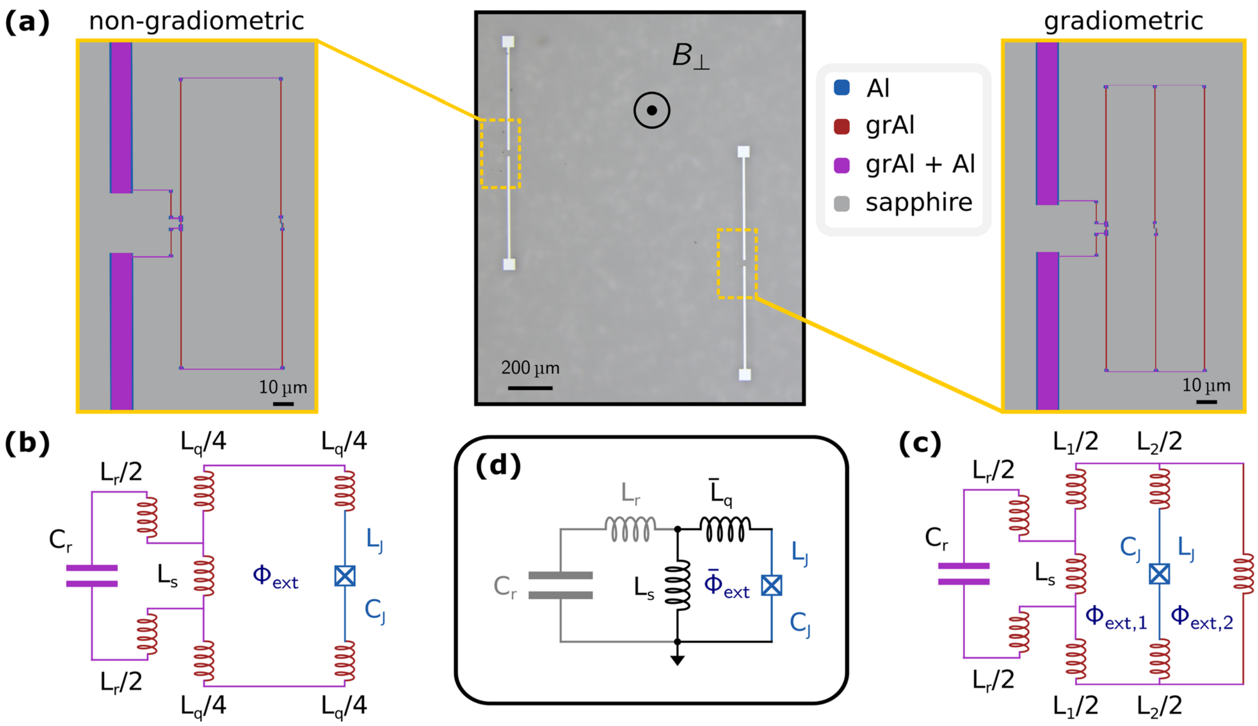

FIG. 1. Gradiometric fluxonium. (a) Optical microscopy images of our device, consisting of a pair of fluxonium artificial atoms (central panel)—a non-gradiometric fluxonium with a single loop (left panel) used to calibrate the external magnetic field, roughly 1 mm apart from a fluxonium with gradiometric loop (right panel). In both artificial atoms, a single JJ is shunted by a superinductor made out of grAl similar to Ref. 24. The false colors indicate regions in which pure Al (blue), grAl (red), and a stack of both (purple) are deposited on a sapphire substrate (grey). For readout, the atoms are dispersively coupled to dedicated linear modes via a shared inductance. (b) Effective circuit diagram of the non-gradiometric fluxonium, where C_r and L_r are the capacitance and inductance associated with the linear readout mode, respectively; L_s is the shared inductance; L_q is the atom's loop inductance; and L_J and C_J are the Josephson inductance and capacitance, respectively. **(c)** Effective circuit diagram of the gradiometric fluxonium. The JJ is shunted by two superinductors, forming three loops in total. The flux enclosed in the two inner loops is $\Phi_{ext,1}$ and $\Phi_{ext,2}$. (d) Both implementations can be mapped onto a simplified circuit model. While the mapping of the non-gradiometric design is trivial, we find non-trivial expressions for the effective flux bias $\bar{\Phi}_{ext}$ and the effective loop inductance $\bar{L}_q$ for the gradiometric case (see supplementary material S1).

shielded from ionizing radiation. The measured extinction of persistent current in our $50 \times 160\,\mathrm{nm}^2$ cross-sectional grAl wire is reminiscent of the operating principle of transition edge sensors[36] and superconducting nanowire single-photon detectors,[37,38] which, when DC biased, can transition to a dissipative state due to a sudden burst of quasiparticles following an energy absorbing event. We confirm that the escape of trapped flux from the gradiometric loop is related to radioactivity by moving samples to the Gran Sasso National Laboratory (LNGS) underground facility. Here, we measure a significant fluxon lifetime increase, from hours (above ground) to days. In the presence of a ThO_2 radioactive source (same setup as in Ref. 39), this time reduces again to ∼30 minutes.

The sample design, shown in Fig. 1(a), consists of a pair of fluxonium artificial atoms, one with a non-gradiometric and the other with a gradiometric loop geometry, respectively. Both devices are fabricated on a $0.33 \times 10 \times 15\,\mathrm{mm}^3$ c-plane sapphire substrate by means of a three-angle shadow evaporation, similar to Ref. 24 (see S2). The modulation periodicity of the non-gradiometric atom is used to calibrate the external magnetic flux created by a superconducting field coil. Although the devices are around 1 mm apart to reduce electromagnetic interaction, the diameter of the field coil is more than one order of magnitude larger, ensuring a homogeneous field $B_\perp$. For readout, both fluxonium atoms are dispersively coupled to dedicated readout modes by sharing a small fraction of their loop inductance. The capacitor of these two readout modes is designed in the form of a microwave antenna and couples them to the electric field of a 3D copper waveguide sample holder similar to Ref. 24.

For both device geometries, we derive effective lumped-element circuit models [see Fig. 1 panels (b) and (c)]. Since the readout is implemented similarly, the capacitance and inductance of the readout modes are denoted C_r and L_r, respectively, and L_s is the shared inductance. The non-gradiometric design has a single loop with a superinductance L_q shunting the JJ (blue crossed-box symbol). The gradiometric design has two shunt inductances forming three loops: an outer loop with surface area $A = 50 \times 150\,\mu\mathrm{m}^2$, and two inner loops with surface area $A/2$. The inductance in each loop branch is denoted L_i, with the index $i \in \{1, 2, 3\}$ indicating the corresponding branch. The gradiometric atom can be mapped onto the standard fluxonium circuit diagram shown in Fig. 1(d) using an effective flux bias $\bar{\Phi}_{\mathrm{ext}}$ and an effective shunting inductance $\bar{L}_q$ (see S1).

The superconducting field coil is calibrated by measuring the spectrum of the non-gradiometric device, designed with the same loop area A, located on the same substrate. Figure 2(a) depicts the phase response $\arg(S_{11})$ of the readout mode coupled to the non-gradiometric fluxonium atom as a function of the probe frequency f_d and the external magnetic field $B_\perp$, measured in close vicinity of the readout frequency $f_r = 7.445\,\mathrm{GHz}$. The fundamental transition frequency of the fluxonium $f_{01}(\bar{\Phi}_{\mathrm{ext}})$ oscillates between values below and above the readout frequency, resulting in avoided-level-crossings repeated with periodicity of $B_0 = 0.28\,\mu\mathrm{T}$.

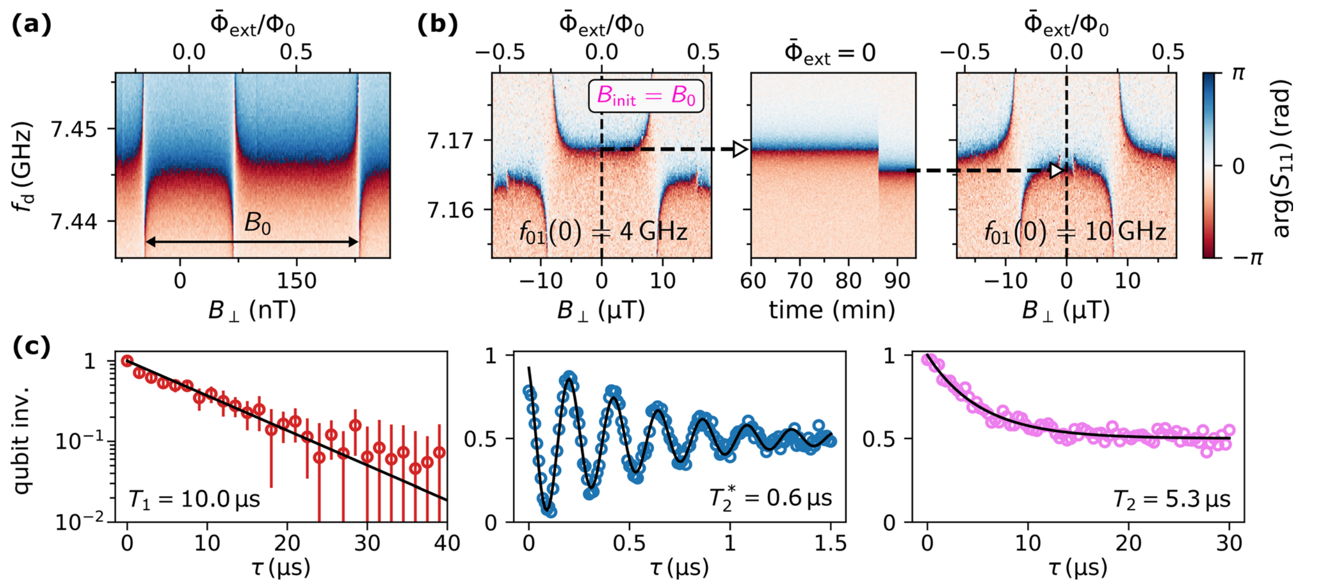

FIG. 2. (a) Calibration of the external field using the periodicity of the non-gradiometric fluxonium spectrum. The colorplot shows the phase of the reflection coefficient $\arg(S_{11})$ of the linear readout mode as a function of the external magnetic field $B_\perp$. The fundamental transition frequency of the fluxonium $f_{01}(\bar{\Phi}_{\mathrm{ext}})$ crosses the readout mode several times, resulting in repeated avoided crossings with a period $B_0 = 280\,\mathrm{nT}$ corresponding to a flux quantum Φ_0 enclosed in the fluxonium loop. (b) Left panel: gradiometric fluxonium initialized at the effective half-flux bias by cooling down in $B_{\mathrm{init}} = B_0$. Notice the factor 120 reduced sensitivity of the gradiometric device to $B_\perp$ in comparison with panel (a). Central panel: the time trace of the phase response measured at $B_\perp = 0$. The corresponding cut is indicated in left panel by a vertical dashed line. The jump of the frequency of the readout mode detected at ≈85 minutes after crossing $T_{\mathrm{c,grAl}} \approx 2\,\mathrm{K}$ corresponds to an escape of the trapped flux. Right panel: gradiometric device after the flux escape. The direction of the avoided crossings demonstrates that the fundamental fluxonium transition is found above (left) and below (right) the readout mode frequency in applied zero-field $B_\perp = 0$. The small avoided crossings visible in the vicinity of $B_\perp = 0$ in the right panel correspond to two-photon transitions. (c) Coherence of the gradiometric fluxonium after half-flux initialization: the qubit population inversion as function of time for energy relaxation (left), Ramsey fringes (center), and Hahn-echo experiment (right). Zero inversion corresponds to the finite population caused by thermal excitations at the fridge temperature of 20 mK and other non-equilibrium processes. The black lines indicate the numerical fit of the data (markers). Error bars in left panel show the measured standard deviation.

The gradiometric fluxonium can be initialized at the half-flux effective bias by cooling the device down through the metal-to-superconductor phase transition in a static magnetic field $B_{init} = B_0$ corresponding to a single flux quantum enclosed in the outer fluxonium loop (see S3). The magnetic field is ramped down at the base temperature of the cryogenic refrigerator (20 mK), well below the critical temperature $T_{c,grAl} \approx 2$ K of the grAl film. However, the enclosed flux is now trapped in the gradiometric loop. In the case of perfectly symmetric inner loops and zero field gradient, the phase difference across the JJ equals π, pinning the atom at the half-flux bias. Figure 2(b) shows the gradiometric fluxonium after initialization at the effective half-flux bias (left panel). Wide range flux sweeps of the gradiometric device are shown in S5. The difference in field range covered in Figs. 2(a) and 2(b) illustrates the suppression of global magnetic field sensitivity by roughly a factor of 120 for the gradiometric fluxonium. According to our effective circuit model, the remaining field sensitivity could be either caused by an asymmetry of the outer loop inductances or by a small field gradient.

Figure 2(c) depicts time-domain characterization of the coherence properties of the gradiometric atom. For the gradiometric fluxonium initialized at the effective half-flux bias, we find a Ramsey coherence time of $T_2^\star = 0.59 \pm 0.02\,\mu$s, which is not limited by the energy relaxation time $T_1 = 10.0 \pm 0.3\,\mu$s. We measured T_1 fluctuations of 10% on a timescale of two hours. Notably, the non-gradiometric fluxonium located on the same chip exhibits similar coherence times $T_1 = 2.5 \pm 0.3\,\mu$s and $T_2^\star = 0.76 \pm 0.04\,\mu$s, which excludes the gradiometric geometry as the cause of the much smaller coherence compared to previous fluxonium implementations based on similar grAl superinductors.[24] Moreover, in both devices, we do not observe an improvement in coherence around the half-flux sweet spot (see S4). While the sensitivity to homogeneous fields is decreased for the gradiometric device, this is not the case for local flux noise, which might even increase due to larger length of the shunting inductance.[40] A single spin echo pulse improves the coherence by almost an order of magnitude for the gradiometric fluxonium, up to $T_2 = 5.3 \pm 0.3\,\mu$s, and by a factor of 3.5 for the non-gradiometric fluxonium, up to $T_2 = 2.6 \pm 0.4\,\mu$s. Therefore, we conclude that Ramsey coherence of all devices on this chip is limited by local and low-frequency noise of unknown origin.

The time stability of the half-flux initialization is determined by fluxon escape rate, which becomes apparent by an abrupt change in persistent current under constant or zero magnetic field bias. To suppress fluxon dynamics, the outer loop of gradiometric devices needs to be implemented using a superconducting wire with a low phase slip rate. The expected phase slip rate in our grAl superinductance can be found by modeling the material as an effective array of JJs.[41] The calculated phase-slip rate is $\sim 10^{-20}$ Hz (see S5). In strong contrast, in all four cooldowns in the cryostat located in Karlsruhe (not shielded from ionizing radiation), we observe an escape of the trapped flux once in a few hours, similar to the phase slip rate found in conventional JJ array superinductors.[19] The time evolution of the readout mode in Fig. 2(b) shows a detected flux escape event, manifesting as a frequency jump at $\approx$85 min after crossing $T_{c,grAl}$. In order to test whether these jumps are caused by ionizing radiation,[42–46] we measure three similar gradiometric devices in the LNGS deep-underground facility (Fig. 3), which was previously used to quantify non-equilibrium quasiparticle poisoning in superconducting quantum circuits.[39] For all devices measured in LNGS, the trapped flux remains stable on a timescale of days. Exposing the cryostat to a ThO_2 radioactive source leads to uncorrelated flux tunneling events and reduces fluxon lifetime to approximately half an hour. The fluxon stability is restored after removal of the source.

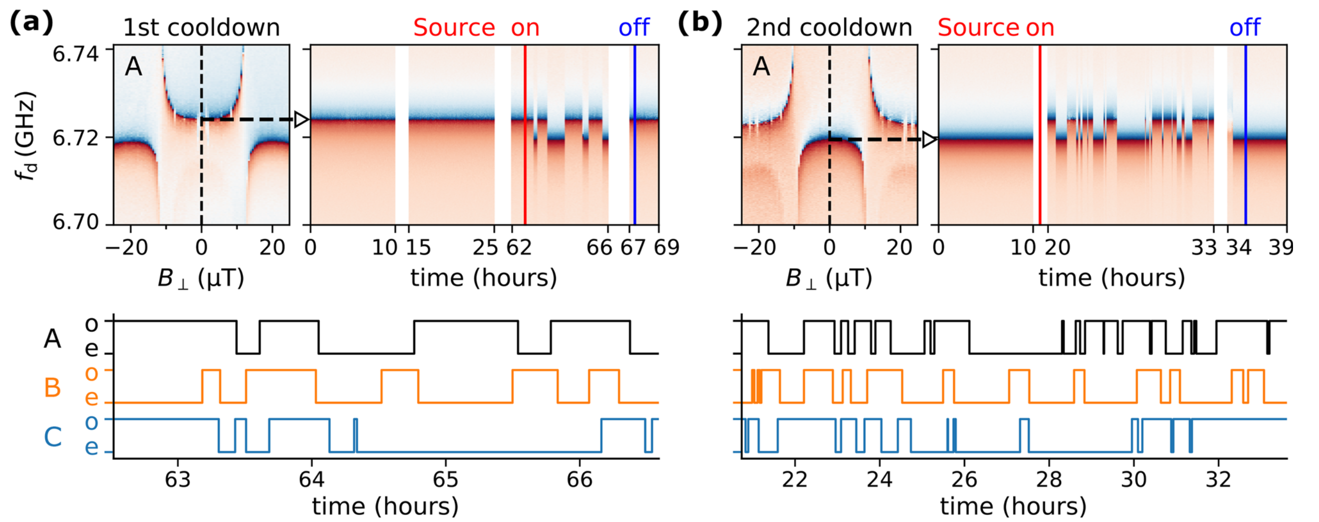

FIG. 3. Fluxon dynamics measured deep-underground in LNGS. The LNGS cryostat is located under a 1.4 km granite overburden (3.6 km water equivalent) and is additionally protected from ionizing radiation with lead shields located both inside and outside the refrigerator. We measured a chip with three gradiometric devices (labeled A, B and C) to check correlations between flux tunneling events. Top panels: the left-hand panels in (a) and (b) show the field dependence of device A in two separate cooldowns demonstrating odd and even state initialization, respectively. The right-hand panels show time traces measured at $B_\perp = 0$. Notice the stability of the trapped flux on timescales of days, before exposing the cryostat to a ThO_2 radioactive source (red vertical line), which activates fluxon dynamics. The blue vertical line indicates source removal. The bottom panels show measured switching dynamics between odd and even states for all devices during ThO_2 exposure.

In summary, we have demonstrated the implementation of a superconducting fluxonium artificial atom with a gradiometric loop geometry, which is two orders of magnitude less sensitive to global magnetic fields compared to a standard, non-gradiometric device with similar loop area. We can initialize our device at the half-flux sweet spot by inducing a persistent current into the outer loop when cooling it down through the metal-to-superconductor transition in a static external magnetic field of $B_{\mathrm{init}} = 0.28\,\mu\mathrm{T}$, equivalent to a single flux quantum enclosed in the outer loop. From pulsed time-domain measurements, we find that the coherence of the gradiometric device is comparable to that of regular fluxoniums on the same chip, and it is limited by local, low-frequency noise, which can be filtered by a single spin echo pulse.

Although the superinductor in our device is implemented using superconducting grAl, which is expected to have a significantly smaller phase-slip rate compared to conventional JJ arrays,[19] we observe a similar escape rate of the flux after half-flux initialization, which is indicative of catastrophic events, for instance, caused by radioactive or cosmic impacts locally weakening superconductivity in the outer loop wire. Indeed, we confirm this hypothesis by measuring order of magnitude increased lifetimes of trapped fluxons in the LNGS deep-underground facility. Our results add another item to the list of detrimental effects of ionizing radiation in superconducting hardware and provide additional motivation to implement radiation mitigation.[39,45,47–49]

See the supplementary material for the Hamiltonian of gradiometric fluxonium, sample fabrication, gradiometric fluxonium initialization at half flux bias, measured spectrum and coherence of the gradiometric fluxonium, and escape of the trapped flux from grAl loop.

The authors are grateful to L. Grünhaupt for fruitful discussions, and they acknowledge technical support from S. Diewald, A. Lukashenko, and L. Radtke. Funding is provided by the Alexander von Humboldt foundation in the framework of a Sofja Kovalevskaja award endowed by the German Federal Ministry of Education and Research and by the European Union's Horizon 2020 programme under No. 899561 (AVaQus). P.P. and I.M.P. acknowledge support from the German Ministry of Education and Research (BMBF) within the QUANTERA project SiUCs (FKZ: 13N15209). L.P.Z and L-M. P-Ţ. acknowledge the Romanian National Authority for Scientific Research and Innovation, CNCS-UEFISCDI for funding through the project PCCF Project No. PN-III-P4-ID-PCCF-2016-0047 and the project Quantum Computation with Schrödinger cat states, contract ERANET-QUANTERA-QuCos 120/16.09.2019. S.G., D.R. and W.W. acknowledge support from the European Research Council advanced grant MoQuOS (N. 741276). The facilities use were supported by the KIT Nanostructure Service Laboratory (NSL). They acknowledge qKit for providing a convenient measurement software framework. They thank the director and technical staff of INFN-LNGS and the LNGS Computing and Network Service for their support. They are grateful to M. Guetti and M. Iannone for the support with construction of the cryogenic setup at LNGS. The work was supported by INFN and by the U.S. Department of Energy, Office of Science, National Quantum Information Science Research Centers, Superconducting Quantum Materials and Systems Center (SQMS) under Contract No. DE-AC02-07CH11359.

AUTHOR DECLARATIONS

Conflict of Interest

The authors declare that there is no conflicts of interest.

DATA AVAILABILITY

The data that support the findings of this study are available from the corresponding author upon reasonable request.

REFERENCES

[1] J. Zmuidzinas and P. Richards, "Superconducting detectors and mixers for millimeter and submillimeter astrophysics," Proc. IEEE **92**, 1597 (2004).
[2] K. Irwin and G. Hilton, "Transition-edge sensors," in *Cryogenic Particle Detection*, edited by C. Enss (Springer, Berlin/Heidelberg, 2005), pp. 63–150.
[3] B. A. Mazin, "Microwave kinetic inductance detectors: The first decade," AIP Conf. Proc. **1185**, 135 (2009).
[4] C. M. Natarajan, M. G. Tanner, and R. H. Hadfield, "Superconducting nanowire single-photon detectors: Physics and applications," Superconductor Sci. Technol. **25**, 063001 (2012).
[5] M. A. Castellanos-Beltran, K. D. Irwin, G. C. Hilton, L. R. Vale, and K. W. Lehnert, "Amplification and squeezing of quantum noise with a tunable Josephson metamaterial," Nat. Phys. **4**, 929 (2008).
[6] N. Bergeal, F. Schackert, M. Metcalfe, R. Vijay, V. E. Manucharyan, L. Frunzio, D. E. Prober, R. J. Schoelkopf, S. M. Girvin, and M. H. Devoret, "Phase-preserving amplification near the quantum limit with a Josephson ring modulator," Nature **465**, 64 (2010).
[7] A. Roy and M. Devoret, "Introduction to parametric amplification of quantum signals with Josephson circuits," C. R. Phys. **17**, 740 (2016).
[8] M. H. Devoret and R. J. Schoelkopf, "Superconducting circuits for quantum information: An outlook," Science **339**, 1169 (2013).
[9] G. Wendin, "Quantum information processing with superconducting circuits: A review," Rep. Prog. Phys. **80**, 106001 (2017).
[10] Z.-L. Xiang, S. Ashhab, J. Q. You, and F. Nori, "Hybrid quantum circuits: Superconducting circuits interacting with other quantum systems," Rev. Mod. Phys. **85**, 623 (2013).
[11] Y. B. Kim, C. F. Hempstead, and A. R. Strnad, "Critical persistent currents in hard superconductors," Phys. Rev. Lett. **9**, 306 (1962).
[12] W. A. Little, "Decay of persistent currents in small superconductors," Phys. Rev. **156**, 396 (1967).
[13] K. Likharev and V. Semenov, "RSFQ logic/memory family: A new josephson-junction technology for sub-terahertz-clock-frequency digital systems," IEEE Trans. Appl. Supercond. **1**, 3 (1991).
[14] P. Bunyk, K. Likharev, and D. Zinoviev, "RSFQ technology: Physics and devices," Int. J. High Speed Electron. Syst. **11**, 257 (2001).
[15] J. B. Majer, J. R. Butcher, and J. E. Mooij, "Simple phase bias for superconducting circuits," Appl. Phys. Lett. **80**, 3638 (2002).
[16] S. Backens, A. Shnirman, Y. Makhlin, Y. Gefen, J. E. Mooij, and G. Schön, "Emulating majorana fermions and their braiding by ising spin chains," Phys. Rev. B **96**, 195402 (2017).
[17] A. Petrescu, H. E. Türeci, A. V. Ustinov, and I. M. Pop, "Fluxon-based quantum simulation in circuit QED," Phys. Rev. B **98**, 174505 (2018).
[18] M. T. Bell, I. A. Sadovskyy, L. B. Ioffe, A. Y. Kitaev, and M. E. Gershenson, "Quantum superinductor with tunable nonlinearity," Phys. Rev. Lett. **109**, 137003 (2012).
[19] N. A. Masluk, I. M. Pop, A. Kamal, Z. K. Minev, and M. H. Devoret, "Microwave characterization of Josephson junction arrays: Implementing a low loss superinductance," Phys. Rev. Lett. **109**, 137002 (2012).
[20] M. Peruzzo, A. Trioni, F. Hassani, M. Zemlicka, and J. M. Fink, "Surpassing the resistance quantum with a geometric superinductor," Phys. Rev. Appl. **14**, 044055 (2020).
[21] V. E. Manucharyan, J. Koch, L. I. Glazman, and M. H. Devoret, "Fluxonium: Single cooper-pair circuit free of charge offsets," Science **326**, 113 (2009).

[22] I. M. Pop, K. Geerlings, G. Catelani, R. J. Schoelkopf, L. I. Glazman, and M. H. Devoret, "Coherent suppression of electromagnetic dissipation due to superconducting quasiparticles," Nature **508**, 369 (2014).
[23] A. Somoroff, Q. Ficheux, R. A. Mencia, H. Xiong, R. V. Kuzmin, and V. E. Manucharyan, "Millisecond coherence in a superconducting qubit," arXiv:2103.08578 [quant-ph] (2021).
[24] L. Grünhaupt, M. Spiecker, D. Gusenkova, N. Maleeva, S. T. Skacel, I. Takmakov, F. Valenti, P. Winkel, H. Rotzinger, W. Wernsdorfer, A. V. Ustinov, and I. M. Pop, "Granular aluminium as a superconducting material for high-impedance quantum circuits," Nat. Mater. **18**, 816 (2019).
[25] G. Deutscher, H. Fenichel, M. Gershenson, E. Grünbaum, and Z. Ovadyahu, "Transition to zero dimensionality in granular aluminum superconducting films," J. Low Temp. Phys. **10**, 231 (1973).
[26] F. Levy-Bertrand, T. Klein, T. Grenet, O. Dupré, A. Benoît, A. Bideaud, O. Bourrion, M. Calvo, A. Catalano, A. Gomez, J. Goupy, L. Grünhaupt, U. v. Luepke, N. Maleeva, F. Valenti, I. M. Pop, and A. Monfardini, "Electrodynamics of granular aluminum from superconductor to insulator: Observation of collective superconducting modes," Phys. Rev. B **99**, 094506 (2019).
[27] M. J. Schwarz, J. Goetz, Z. Jiang, T. Niemczyk, F. Deppe, A. Marx, and R. Gross, "Gradiometric flux qubits with a tunable gap," New J. Phys. **15**, 045001 (2013).
[28] M. Pita-Vidal, A. Bargerbos, C.-K. Yang, D. J. van Woerkom, W. Pfaff, N. Haider, P. Krogstrup, L. P. Kouwenhoven, G. de Lange, and A. Kou, "Gate-tunable field-compatible fluxonium," Phys. Rev. Appl. **14**, 064038 (2020).
[29] Y. Kubo, C. Grezes, A. Dewes, T. Umeda, J. Isoya, H. Sumiya, N. Morishita, H. Abe, S. Onoda, T. Ohshima, V. Jacques, A. Dréau, J.-F. Roch, I. Diniz, A. Auffeves, D. Vion, D. Esteve, and P. Bertet, "Hybrid quantum circuit with a superconducting qubit coupled to a spin ensemble," Phys. Rev. Lett. **107**, 220501 (2011).
[30] V. Ranjan, G. de Lange, R. Schutjens, T. Debelhoir, J. P. Groen, D. Szombati, D. J. Thoen, T. M. Klapwijk, R. Hanson, and L. DiCarlo, "Probing dynamics of an electron-spin ensemble via a superconducting resonator," Phys. Rev. Lett. **110**, 067004 (2013).
[31] N. Samkharadze, G. Zheng, N. Kalhor, D. Brousse, A. Sammak, U. C. Mendes, A. Blais, G. Scappucci, and L. M. K. Vandersypen, "Strong spin-photon coupling in silicon," Science **359**, 1123 (2018).
[32] X. Mi, M. Benito, S. Putz, D. M. Zajac, J. M. Taylor, G. Burkard, and J. R. Petta, "A coherent spin-photon interface in silicon," Nature **555**, 599 (2018).
[33] L. Bogani and W. Wernsdorfer, "Molecular spintronics using single-molecule magnets," Nat. Mater. **7**, 179 (2008).
[34] W. Wernsdorfer and M. Ruben, "Synthetic Hilbert space engineering of molecular qudits: Isotopologue chemistry," Adv. Mater. **31**, 1806687 (2019).
[35] A. Kou, W. C. Smith, U. Vool, R. T. Brierley, H. Meier, L. Frunzio, S. M. Girvin, L. I. Glazman, and M. H. Devoret, "Fluxonium-based artificial molecule with a tunable magnetic moment," Phys. Rev. X **7**, 031037 (2017).
[36] K. D. Irwin, "An application of electrothermal feedback for high resolution cryogenic particle detection," Appl. Phys. Lett. **66**, 1998 (1995).
[37] G. N. Gol'tsman, O. Okunev, G. Chulkova, A. Lipatov, A. Semenov, K. Smirnov, B. Voronov, A. Dzardanov, C. Williams, and R. Sobolewski, "Picosecond superconducting single-photon optical detector," Appl. Phys. Lett. **79**, 705 (2001).
[38] B. Korzh, Q.-Y. Zhao, J. P. Allmaras, S. Frasca, T. M. Autry, E. A. Bersin, A. D. Beyer, R. M. Briggs, B. Bumble, M. Colangelo, G. M. Crouch, A. E. Dane, T. Gerrits, A. E. Lita, F. Marsili, G. Moody, C. Peña, E. Ramirez, J. D. Rezac, N. Sinclair, M. J. Stevens, A. E. Velasco, V. B. Verma, E. E. Wollman, S. Xie, D. Zhu, P. D. Hale, M. Spiropulu, K. L. Silverman, R. P. Mirin, S. W. Nam, A. G. Kozorezov, M. D. Shaw, and K. K. Berggren, "Demonstration of sub-3 ps temporal resolution with a superconducting nanowire single-photon detector," Nat. Photonics **14**, 250 (2020).
[39] L. Cardani, F. Valenti, N. Casali, G. Catelani, T. Charpentier, M. Clemenza, I. Colantoni, A. Cruciani, G. D'Imperio, L. Gironi, L. Grünhaupt, D. Gusenkova, F. Henriques, M. Lagoin, M. Martinez, G. Pettinari, C. Rusconi, O. Sander, C. Tomei, A. V. Ustinov, M. Weber, W. Wernsdorfer, M. Vignati, S. Pirro, and I. M. Pop, "Reducing the impact of radioactivity on quantum circuits in a deep-underground facility," Nat. Commun. **12**, 2733 (2021).
[40] T. Lanting, A. J. Berkley, B. Bumble, P. Bunyk, A. Fung, J. Johansson, A. Kaul, A. Kleinsasser, E. Ladizinsky, F. Maibaum, R. Harris, M. W. Johnson, E. Tolkacheva, and M. H. S. Amin, "Geometrical dependence of the low-frequency noise in superconducting flux qubits," Phys. Rev. B **79**, 060509 (2009).
[41] N. Maleeva, L. Grünhaupt, T. Klein, F. Levy-Bertrand, O. Dupre, M. Calvo, F. Valenti, P. Winkel, F. Friedrich, W. Wernsdorfer, A. V. Ustinov, H. Rotzinger, A. Monfardini, M. V. Fistul, and I. M. Pop, "Circuit quantum electrodynamics of granular aluminum resonators," Nat. Commun. **9**, 3889 (2018).
[42] L. J. Swenson, A. Cruciani, A. Benoit, M. Roesch, C. S. Yung, A. Bideaud, and A. Monfardini, "High-speed phonon imaging using frequency-multiplexed kinetic inductance detectors," Appl. Phys. Lett. **96**, 263511 (2010).
[43] L. Grünhaupt, N. Maleeva, S. T. Skacel, M. Calvo, F. Levy-Bertrand, A. V. Ustinov, H. Rotzinger, A. Monfardini, G. Catelani, and I. M. Pop, "Loss mechanisms and quasiparticle dynamics in superconducting microwave resonators made of thin-film granular aluminum," Phys. Rev. Lett. **121**, 117001 (2018).
[44] A. P. Vepsäläinen, A. H. Karamlou, J. L. Orrell, A. S. Dogra, B. Loer, F. Vasconcelos, D. K. Kim, A. J. Melville, B. M. Niedzielski, J. L. Yoder, S. Gustavsson, J. A. Formaggio, B. A. VanDevender, and W. D. Oliver, "Impact of ionizing radiation on superconducting qubit coherence," Nature **584**, 551 (2020).
[45] M. McEwen, L. Faoro, K. Arya, A. Dunsworth, T. Huang, S. Kim, B. Burkett, A. Fowler, F. Arute, J. C. Bardin, A. Bengtsson, A. Bilmes, B. B. Buckley, N. Bushnell, Z. Chen, R. Collins, S. Demura, A. R. Derk, C. Erickson, M. Giustina, S. D. Harrington, S. Hong, E. Jeffrey, J. Kelly, P. V. Klimov, F. Kostritsa, P. Laptev, A. Locharla, X. Mi, K. C. Miao, S. Montazeri, J. Mutus, O. Naaman, M. Neeley, C. Neill, A. Opremcak, C. Quintana, N. Redd, P. Roushan, D. Sank, K. J. Satzinger, V. Shvarts, T. White, Z. J. Yao, P. Yeh, J. Yoo, Y. Chen, V. Smelyanskiy, J. M. Martinis, H. Neven, A. Megrant, L. Ioffe, and R. Barends, "Resolving catastrophic error bursts from cosmic rays in large arrays of superconducting qubits," arXiv:2104.05219 (2021).
[46] C. D. Wilen, S. Abdullah, N. A. Kurinsky, C. Stanford, L. Cardani, G. D'Imperio, C. Tomei, L. Faoro, L. B. Ioffe, C. H. Liu, A. Opremcak, B. G. Christensen, J. L. DuBois, and R. McDermott, "Correlated charge noise and relaxation errors in superconducting qubits," Nature **594**, 369 (2021).
[47] K. Karatsu, A. Endo, J. Bueno, P. J. de Visser, R. Barends, D. J. Thoen, V. Murugesan, N. Tomita, and J. J. A. Baselmans, "Mitigation of cosmic ray effect on microwave kinetic inductance detector arrays," Appl. Phys. Lett. **114**, 032601 (2019).
[48] F. Henriques, F. Valenti, T. Charpentier, M. Lagoin, C. Gouriou, M. Martínez, L. Cardani, M. Vignati, L. Grünhaupt, D. Gusenkova, J. Ferrero, S. T. Skacel, W. Wernsdorfer, A. V. Ustinov, G. Catelani, O. Sander, and I. M. Pop, "Phonon traps reduce the quasiparticle density in superconducting circuits," Appl. Phys. Lett. **115**, 212601 (2019).
[49] J. M. Martinis, "Saving superconducting quantum processors from qubit decay and correlated errors generated by gamma and cosmic rays," arXiv:2012.06137 [quant-ph] (2021).